

Statistical theory of cumulant mapping in an imperfect apparatus

S. Patchkovskii^{1,*} and J. Mikosch^{2,†}

¹*Max-Born-Institute, Max-Born-Str. 2A, 12489 Berlin, Germany*

²*Institut für Physik, Universität Kassel, Heinrich-Plett-Str. 40, 34132 Kassel, Germany*

(Dated: December 25, 2024)

Cumulant mapping has been recently suggested [Frasinski, Phys. Chem. Chem. Phys. **24**, 207767 (2022)] as an efficient approach to observing multi-particle fragmentation pathways, while bypassing the restrictions of the usual coincidence-measurement approach. We present a formal analysis of the cumulant-mapping technique in the presence of moderate external noise, which induces spurious correlations between the fragments. Suppression of false-cumulant signal may impose severe restrictions on the stability of the experimental setup and/or the permissible average event rate, which increase with the cumulant order. We outline the constraints on the process being investigated, which allow cumulant mapping to remain competitive in the presence of external noise. We further propose a simple test for false-cumulant detection, based on the power-law relationship between the average event rate and the cumulant.

I. INTRODUCTION

Covariance mapping[1] is an ingenious statistical analysis of multi-particle fragmentation experiments, which allows fragment correlations to be established without a restriction of a single event per measurement shot, and with only moderate requirements for the fragment detection efficiency. Covariance-based measurements can often reach statistical significance in a fraction of time[2], which would have been required for the more traditional[3] coincidence-based approaches. Covariance mapping has enabled remarkable advances in experiments where isolated molecules are broken up, such as X-ray and strong-field induced dissociation and Coulomb Explosion Imaging of small molecules[4–6], in particular with ultra-bright Free Electron Lasers (FELs) [7–10] - including pump-probe studies of molecular dynamics[11–13]. Covariance mapping is constantly further conceptually refined[14, 15] and adopted for structure determination of more complex systems, such as isolated biomolecules via collision-induced fragmentation[16], as well as imaging of tetracene dimers formed inside[17] and of alkali trimers produced on the surface of[18] helium nanodroplets via femtosecond laser-induced Coulomb explosion. Recently, an extension of the covariance mapping to multiparticle correlations, the cumulant mapping, has been proposed[19]. First experimental realization of the technique have already appeared[20], as well as mathematical refinements of the statistical treatment[21, 22].

The Achilles’ heel of the covariance-mapping techniques are the spurious correlations between fragments, induced by external fluctuations in experimental parameters, such as the target density or the laser pulse fluence and/or intensity[23–25]. Such fluctuations are an inevitable consequence of experimental imperfections, and induce “false” covariances between all fragments, poten-

tially swamping weak channels of interest. If an independent, shot-by-shot measurement of the fluctuating parameter is available[26, 27], their effect can be reversed using “partial” covariances[28]. Alternatively, simultaneous detection of a sufficient number of fragmentation channels can be used to implement a *self-correcting* partial covariance[29], even when no explicit measurement of the fluctuating external parameter(s) is available.

A statistical analysis of covariance measurement in an imperfect apparatus, placing constraints on the permissible noise level and event rates, has been available in the literature for some time[23, 24]. Unfortunately, we are not aware of a comparable investigation of the cumulant mapping. The goal of this contribution is to fill this lacuna, using techniques developed in Ref. [23] and previously applied to the analysis of self-correcting covariances[29].

The rest of this work is organized as follows: Section II demonstrates the appearance of “false” covariances in a 3-cumulant via a numerical experiment, Section III establishes notation and recapitulates key results from Ref. [23], necessary to follow the discussion. Section IV presents the expectations and the variances of the 2-, 3-, and 4-cumulants in an imperfect apparatus. Section V discusses the constraints imposed by these results on the experimental parameters, in a number of typical scenarios. Finally, section VI summarized the work and offers the outlook for future developments.

II. THE PRELUDE: NUMERICAL EXPERIMENT

To illustrate the appearance of “false” cumulants due to noise-induced correlations, we perform a numerical Monte-Carlo simulation, fashioned after a realistic experimental situation. A generic triatomic molecule, ABC, breaks up via Coulomb Explosion Imaging driven by an ultrashort, intense infrared or X-ray laser pulse, which ionizes the molecule. The desired channel, delivering structural information, is the complete fragmentation

* serguei.patchkovskii@mbi-berlin.de

† mikosch@uni-kassel.de

into $A^+ + B^+ + C^+$. This channel is assumed to be weak – we adopt statistical probability of 1%. The incomplete fragmentation channels $A^+ + BC^+$, $AC^+ + B^+$, and $AB^+ + C^+$ are taken to be much more likely. For simplicity, and without qualitatively affecting our conclusions, we assume that each of these incomplete channels occurs with an equal statistical probability of 33%.

The benefit of covariance over coincidence detection is to be able to perform an experiment in a regime where multiple break-up events occur per laser shot. In our simulation, the number of break-up events per shot is drawn from a noise-augmented Poisson distribution. As is more rigorously put in equations in the following section, the noise implies that the average event rate ν of a Poisson distribution is no longer a fixed parameter, but is instead sampled from normal distribution with the mean ν_0 and standard deviation $\gamma\nu_0$. For simplicity, we initially assume an unrealistic detection efficiency for fragments of $\beta = 100\%$. Note that in the terminology used by Frasiniski[19], this numerical experiment is entirely “noise-free”, since no undesired correlated fragmentation pathways are present.

We used $N = 5 \times 10^7$ shots for each simulation, which we repeated 10 times to obtain the average of the 3-cumulant and its standard deviation. The noise parameter γ , the number of events per shot ν , the fragmentation channel assigned to each event, and whether the individual fragments are detected (for $\beta < 100\%$) are all independently statistically determined, via drawing random numbers from Gaussian, Poissonian, and uniform distributions. In each simulation, we loop through the N shots twice - once to determine the average rates and a second time to calculate the 3-cumulant. Importantly, the same pseudo-random numbers are used in the two passes of the simulation, ensured by using the same random seed - which is otherwise randomly generated for each simulation. Since the simulation is carried out event-by-event, we can determine not only the overall 3-cumulant, but also the “true” 3-cumulant, which results from the desired three-body fragmentation channel.

In Fig.1(a), the numerically measured 3-cumulant κ_3 is plotted as a function of the average event rate ν_0 , for standard deviations σ of the noise distribution of 0.1 (10% noise / red squares) and 0.3 (30% noise / blue triangles). The “true” 3-cumulant is plotted as black circles. Error bars represent 10 standard deviations, and are in most cases below the size of the markers. Dashed lines connect the simulation results for visual guidance. The “true” 3-cumulant, stemming from the desired triple-fragmentation events alone, is found to increase linearly with average event rate ν_0 . At the same time, the relative statistical error is found to decrease with ν_0 . This observation represents the “covariance advantage”. In the absence of noise, the 3-cumulant κ_3 is a strongly increased correlation signal, as compared to the coincidence detection regime which requires $\nu_0 \ll 1$ to avoid false coincidences.

However, Fig.1(a) also shows how the “true” 3-

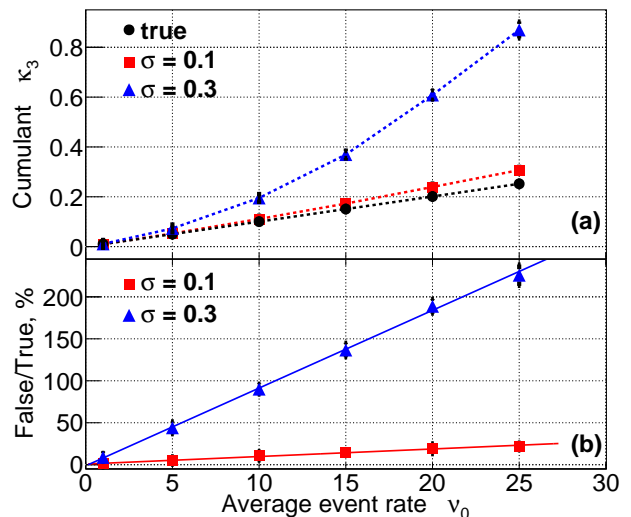


FIG. 1. Results of a numerical Monte-Carlo simulation, demonstrating how external noise, such as shot-to-shot fluctuations of laser power or pulse duration, leads to very significant deviations of the cumulant observable from the true value. The situation in the simulation represents a minor process with strong, but uncorrelated background - the three-body breakup of a molecule ABC into $A + B + C$ (1% probability), with background from $A + BC$, $AC + B$, and $AB + C$ (33% probability each).

cumulant of the desired three-body fragmentation channel is increasingly “polluted” by the coincidental two-body fragmentation channels with increasing noise. For larger σ , κ_3 deviates increasingly from the linear dependence on ν_0 , eventually coming to dominate the signal. Also the relative error is strongly increased, as can be seen from the appearance of error bars that are larger than the marker size. In Fig. 1(b) the ratio of false to true κ_3 extracted from the data in panel (a) is displayed, along with linear fits. This ratio, marking the systematic error to the desired “true” 3-cumulant, is found to increase linearly with average event rate ν_0 , and the slope is strongly increased for $\sigma = 0.3$ as compared to $\sigma = 0.1$.

The simulation was repeated for a reduced detection efficiency, $\beta = 0.5$ (50% fragment detection probability). We observe that 3-cumulant is reduced by β^3 and that its relative error is increased. The ratio of false to true 3-cumulant, however, stays the same, albeit with a larger statistical error.

The results of the numerical experiment as shown in Fig.1 caution that in covariance detection the average event rate ν_0 has to be kept below a limit that is given by a systematic error to the n-cumulant that is deemed tolerable. This issue arises when external noise is present, such as statistical fluctuations of the laser power or pulse duration - an omnipresent situation in real experiments, in particular with FELs. The systematic error by “false” covariances strongly increases for increasing noise, which can restrict the beneficial range of an average event rates ν_0 severely. Thus motivated, we are now ready to turn

to a more formal analysis.

III. NOTATION

We consider fragmentation of independent particles, possibly of different kinds, triggered by an external event (a “shot”, such as a light pulse). Each primitive event produces fragments of interest ($1 = X$, $2 = Y$, $3 = Z$, $4 = U$, etc.), plus possibly additional fragments of no concern to us. A fragment label is understood to include not only the intrinsic nature of the particle, but also any relevant bin label assigned in the data analysis. For example, if a water molecule H_2O is Coulomb-exploded in the experiment, we could assign label x to O^+ ions, label Y to H^+ ions with the kinetic energy below 1 eV, and label z to H^+ ions with the kinetic energy above 4 eV.

In each shot, the probability $P(n)$ of n independent fragmentation events occurring follows noise-augmented Poisson distribution[23]:

$$P_\nu(n) = \frac{1}{n!} \nu^n \exp(-\nu), \quad (1)$$

where the primitive event rate $\nu = \nu_0 \gamma$ is sampled from a normal distribution of the relative width σ , centered about the average rate ν_0 :

$$P_\sigma(\gamma) = \frac{1}{\sqrt{2\pi}\sigma} \exp\left(-\frac{(\gamma - 1)^2}{2\sigma^2}\right). \quad (2)$$

We assume that σ is sufficiently small, so that $P_\sigma(\gamma < 0)$, and therefore the probability of (unphysical) negative event rates, is negligible.

Possible outcomes of each elementary event (e.g. detection of particles X and U) are assumed to be mutually-exclusive. Each elementary outcome is described by the corresponding probability P_i . The probability vector of all m relevant outcomes is denoted \mathbb{P} . Similarly, in each shot the fragment counts are given by elements of a vector \mathbb{N} . The moments $M(\mathbb{K})$ of the probability distribution $P(\mathbb{N})$ are defined as:

$$M(\mathbb{K}) = \sum_{n_1=0}^{\infty} \dots \sum_{n_m=0}^{\infty} P(\mathbb{N}) \prod_{i=1}^m n_i^{k_i}. \quad (3)$$

The moments $M(\mathbb{K})$ can be conveniently evaluated using a recursive expression, derived in[23]:

$$M(\mathbb{K} + \mathbb{I}_j) = P_j \nu_0 M(\mathbb{K}) + P_j \frac{\partial}{\partial P_j} M(\mathbb{K}) + \nu_0^2 \sigma^2 P_j \sum_{l=1}^m P_l \sum_{b_l=0}^{k_l-1} \binom{k_l}{b_l} M(\mathbb{K} + \mathbb{I}_l (b_l - k_l)), \quad (4)$$

$$M(\mathbf{0}) = 1, \quad (5)$$

where \mathbb{I}_i denotes a vector of length m , with 1 at position i and zeros at all other indices, and the norm of the distribution $M(\mathbf{0})$ provides the necessary bootstrap.

At the most fundamental level, the fragmentation and detection process are described by the probabilities of fragment formation in an elementary event and their detection in the experimental apparatus. For example, we denote the probability of particles X and Y , and *no other particles of interest*, being produced by a primitive fragmentation event α_{XY} . The corresponding probabilities of detection, once particles are produced, are denoted β_X and β_Y . It is convenient to combine the parameters α and β , which describe the microscopic mechanism of the fragmentation process, into parameters more closely related to the experimental observation. For example, for the case of the 3-particle cumulant, we define:

$$\begin{aligned} \gamma_{XYZ} &= \alpha_{XYZ} \beta_X \beta_Y \beta_Z, \\ \gamma_{XY} &= (\alpha_{XYZ} + \alpha_{XY}) \beta_X \beta_Y, \\ \gamma_{XZ} &= (\alpha_{XYZ} + \alpha_{XZ}) \beta_X \beta_Z, \\ \gamma_{YZ} &= (\alpha_{XYZ} + \alpha_{YZ}) \beta_Y \beta_Z, \\ \gamma_X &= (\alpha_{XYZ} + \alpha_{XY} + \alpha_{XZ} + \alpha_X) \beta_X, \\ \gamma_Y &= (\alpha_{XYZ} + \alpha_{XY} + \alpha_{YZ} + \alpha_Y) \beta_Y, \\ \gamma_Z &= (\alpha_{XYZ} + \alpha_{XZ} + \alpha_{YZ} + \alpha_Z) \beta_Z. \end{aligned} \quad (6)$$

Quantity γ_{XY} of eq. (6), for example, are to be understood as the probability of a single, primitive fragmentation process leading to particles X and Y , plus possibly any other particles, such as Z , being detected.

Clearly, events described by probabilities γ are not mutually-exclusive: detection of particles X , Y , and Z implies that *all other* events in eq. (6) have also occurred. To use these quantities in eq. (4), defined in terms of mutually-exclusive events, we combine them as follows:

$$\begin{aligned} p_{XYZ} &= \gamma_{XYZ}, \\ p_{XY} &= \gamma_{XY} - \gamma_{XYZ}, \\ p_{XZ} &= \gamma_{XZ} - \gamma_{XYZ}, \\ p_{YZ} &= \gamma_{YZ} - \gamma_{XYZ}, \\ p_X &= \gamma_X - \gamma_{XY} - \gamma_{XZ} + \gamma_{XYZ}, \\ p_Y &= \gamma_Y - \gamma_{XY} - \gamma_{YZ} + \gamma_{XYZ}, \\ p_Z &= \gamma_Z - \gamma_{XZ} - \gamma_{YZ} + \gamma_{XYZ}. \end{aligned} \quad (7)$$

From the definitions of the parameters γ , it is easy to convince oneself that probabilities p remain non-negative. They are to be understood as *exclusive* probabilities of observing particles of interest in a primitive fragmentation event. For example, p_{XY} describes probability of particles X and Y , and *no other particles of interest* being observed on the detector. For unit detection efficiency (all $\beta = 1$), quantities p and α coincide.

Because the fragment labels X , Y , etc are entirely arbitrary, all expressions for the expectation and variance of the cumulants must remain symmetric with respect to their permutation. We therefore introduce the symmetrization operator $\mathfrak{S}(Q)$, which transforms its argument Q to a sum of terms with all possible (orderless) permutations of the particle labels, with each term appearing exactly one. Arguments which are already

permutation-symmetric remain unchanged, so that operator \mathfrak{S} is idempotent: $\mathfrak{S}(\mathfrak{S}(Q)) = \mathfrak{S}(Q)$. For example, for the 3-cumulant and particle indices X, Y, and Z:

$$\begin{aligned}\mathfrak{S}(\gamma_{XYZ}) &= \gamma_{XYZ}, \\ \mathfrak{S}(\gamma_X) &= \gamma_X + \gamma_Y + \gamma_Z, \\ \mathfrak{S}(\gamma_{XZ}^2\gamma_Y) &= \gamma_{XZ}^2\gamma_Y + \gamma_{YZ}^2\gamma_X + \gamma_{XY}^2\gamma_Z.\end{aligned}\quad (8)$$

Use of the operator $\mathfrak{S}(Q)$ allows for more compact, and manifestly symmetric, expressions.

Although application of eq. (4) is, in principle, straightforward, for higher-order cumulants it rapidly becomes tedious. Thus, the recursion (4) needs to be invoked 28 times while evaluating the 2-cumulant and its variance, 1198 times for the 3-cumulant and variance, increasing to 370577 times in the case of 4-cumulant. It is therefore best accomplished with the help of a computer-algebra package. We include Mathematica[30] package implementing these derivations as a supplementary material[31], and only give the final results below.

IV. RESULTS

Our main results are presented in the section below. The results for the 2-cumulant (the covariance) were given before[23], in a less symmetric form and under somewhat more restrictive assumptions. In the absence of noise ($\sigma = 0$), for a perfect Poisson source, our results for n -cumulant coincide with those of Frasiniski[19], provided that only the 1- and n -particle fragmentation pathways are considered.

IV.1. 2-cumulant (covariance)

The two fragments of interest are X and Y. The covariance is sampled is sampled from a distribution with the mean κ_2 and variance $\text{Var } \kappa_2$:

$$\begin{aligned}\kappa_2 &= \nu_0\gamma_{XY} + \nu_0^2\sigma^2\gamma_X\gamma_Y, \\ \text{Var } \kappa_2 &= \nu_0\gamma_{XY} + \nu_0^2(\gamma_X\gamma_Y + \gamma_{XY}^2) \\ &\quad + \nu_0^2\sigma^2(\mathfrak{S}(\gamma_X\gamma_{XY}) + \gamma_X\gamma_Y + 2\gamma_{XY}^2) \\ &\quad + \nu_0^3\sigma^2\gamma_X\gamma_Y(\mathfrak{S}(\gamma_X) + 2\gamma_{XY}) \\ &\quad + \nu_0^4\sigma^4(2\gamma_X^2\gamma_Y^2).\end{aligned}\quad (9)$$

IV.2. 3-cumulant

The three fragments of interest are X, Y, and Z. The 3-cumulant κ_3 and its variance are given by:

$$\begin{aligned}\kappa_3 &= \nu_0\gamma_{XYZ} + \nu_0^2\sigma^2\mathfrak{S}(\gamma_{XZ}\gamma_Y), \\ \text{Var } \kappa_3 &= \nu_0\gamma_{XYZ} + \nu_0^2d_{20} + \nu_0^3d_{30} \\ &\quad + \nu_0^2\sigma^2d_{22} + \nu_0^3\sigma^2d_{32} + \nu_0^4\sigma^2d_{42}\end{aligned}\quad (11)$$

$$+ \nu_0^4\sigma^4d_{44} + \nu_0^5\sigma^4d_{54} + \nu_0^6\sigma^6d_{66}, \quad (12)$$

$$\begin{aligned}d_{20} &= 3\gamma_{XYZ}^2 + 4\gamma_{XYZ}\mathfrak{S}(\gamma_{XY}) \\ &\quad + 2\mathfrak{S}(\gamma_{XY}\gamma_{XZ}) + \mathfrak{S}(\gamma_{XZ}\gamma_Y),\end{aligned}\quad (13)$$

$$d_{30} = 8\gamma_{XY}\gamma_{XZ}\gamma_{YZ} + 2\mathfrak{S}(\gamma_{XZ}^2\gamma_Y) + \gamma_X\gamma_Y\gamma_Z, \quad (14)$$

$$\begin{aligned}d_{22} &= 4\gamma_{XYZ}^2 + 2\gamma_{XYZ}(\mathfrak{S}(\gamma_X) + 2\mathfrak{S}(\gamma_{XY})) \\ &\quad + 2\mathfrak{S}(\gamma_{XY}\gamma_{XZ}) + \mathfrak{S}(\gamma_{XZ}\gamma_Y),\end{aligned}\quad (15)$$

$$\begin{aligned}d_{32} &= 24\gamma_{XY}\gamma_{XZ}\gamma_{YZ} + 2\gamma_{XYZ}(2\mathfrak{S}(\gamma_X\gamma_Y) + 7\mathfrak{S}(\gamma_{XZ}\gamma_Y)) \\ &\quad + 8\mathfrak{S}(\gamma_{XZ}(\gamma_X + \gamma_Y)\gamma_{YZ}) + 6\mathfrak{S}(\gamma_{XZ}^2\gamma_Y) \\ &\quad + 4\mathfrak{S}(\gamma_{XY}(\gamma_X + \gamma_Y)\gamma_Z) + \mathfrak{S}(\gamma_{XZ}\gamma_Y^2) \\ &\quad + 3\gamma_X\gamma_Y\gamma_Z,\end{aligned}\quad (16)$$

$$\begin{aligned}d_{42} &= 8\mathfrak{S}(\gamma_X\gamma_{XZ}\gamma_Y\gamma_{YZ}) + 2\mathfrak{S}(\gamma_{XZ}^2\gamma_Y^2) \\ &\quad + \gamma_X\gamma_Y\gamma_Z(\mathfrak{S}(\gamma_X) + 4\mathfrak{S}(\gamma_{XY})),\end{aligned}\quad (17)$$

$$\begin{aligned}d_{44} &= 3\gamma_X\gamma_Y\gamma_Z(\mathfrak{S}(\gamma_X) + 4\mathfrak{S}(\gamma_{XY}) + 8\gamma_{XYZ}) \\ &\quad + 22\mathfrak{S}(\gamma_X\gamma_{XZ}\gamma_Y\gamma_{YZ}) + 5\mathfrak{S}(\gamma_{XZ}^2\gamma_Y^2) \\ &\quad + 6\mathfrak{S}(\gamma_{XY}(\gamma_X + \gamma_Y)\gamma_Z^2),\end{aligned}\quad (18)$$

$$d_{54} = 3\gamma_X\gamma_Y\gamma_Z(\mathfrak{S}(\gamma_X\gamma_Y) + 4\mathfrak{S}(\gamma_{XZ}\gamma_Y)), \quad (19)$$

$$d_{66} = 15\gamma_X^2\gamma_Y^2\gamma_Z^2. \quad (20)$$

IV.3. 4-cumulant

The four fragments of interest are X, Y, Z, U. The 4-cumulant κ_4 and its variance are given by:

$$\begin{aligned}\kappa_4 &= \nu_0\gamma_{XYZU} \\ &\quad + \nu_0^2\sigma^2(\mathfrak{S}(\gamma_U\gamma_{XYZ}) + \mathfrak{S}(\gamma_{XZ}\gamma_{YU})),\end{aligned}\quad (21)$$

$$\begin{aligned}\text{Var } \kappa_4 &= \nu_0\gamma_{XYZU} + \nu_0^2e_{20} + \nu_0^3e_{30} + \nu_0^4e_{40} + \nu_0^2\sigma^2e_{22} \\ &\quad + \nu_0^3\sigma^2e_{32} + \nu_0^4\sigma^2e_{42} + \nu_0^5\sigma^2e_{52} + \nu_0^4\sigma^4e_{44} \\ &\quad + \nu_0^5\sigma^4e_{54} + \nu_0^6\sigma^4e_{64} + \nu_0^6\sigma^6e_{66} \\ &\quad + \nu_0^7\sigma^6e_{76} + \nu_0^8\sigma^8e_{88}.\end{aligned}\quad (22)$$

$$\begin{aligned}e_{20} &= 7\gamma_{XYZU}^2 + \gamma_{XYZU}(4\mathfrak{S}(\gamma_{XU}) + 8\mathfrak{S}(\gamma_{XYU})) \\ &\quad + 4\mathfrak{S}(\gamma_{XYU}\gamma_{XYZ}) + 2\mathfrak{S}(\gamma_{XU}\gamma_{XYZ}) + \mathfrak{S}(\gamma_{XZ}\gamma_{YU}) \\ &\quad + \mathfrak{S}(\gamma_U\gamma_{XYZ}),\end{aligned}\quad (23)$$

$$\begin{aligned}e_{30} &= 14\gamma_{XYZU}\mathfrak{S}(\gamma_{XZ}\gamma_{YU}) + 16\mathfrak{S}(\gamma_{XYZ}\gamma_{XZU}\gamma_{YU}) \\ &\quad + 4\mathfrak{S}(\gamma_U\gamma_{XYZ}^2) + 8\mathfrak{S}(\gamma_{XZU}(\gamma_{XY}\gamma_{YU} + \gamma_{XU}\gamma_{YZ})) \\ &\quad + 4\mathfrak{S}(\gamma_{XU}\gamma_{XZ}\gamma_{YU}) + 4\mathfrak{S}(\gamma_U\gamma_{XY}\gamma_{XYZ}) \\ &\quad + 2\mathfrak{S}(\gamma_{XZ}^2\gamma_{YU}) + 2\mathfrak{S}(\gamma_U\gamma_{XY}\gamma_{XZ}) \\ &\quad + \mathfrak{S}(\gamma_U\gamma_{XZ}\gamma_Y),\end{aligned}\quad (24)$$

$$\begin{aligned}e_{40} &= 3\mathfrak{S}(\gamma_{XZ}^2\gamma_{YU}^2) + 14\mathfrak{S}(\gamma_{XU}\gamma_{XZ}\gamma_{YU}\gamma_{YZ}) \\ &\quad + 8\mathfrak{S}(\gamma_U\gamma_{XY}\gamma_{XZ}\gamma_{YZ}) + 2\mathfrak{S}(\gamma_U\gamma_{XZ}^2\gamma_Y) \\ &\quad + \gamma_U\gamma_X\gamma_Y\gamma_Z,\end{aligned}\quad (25)$$

$$\begin{aligned}e_{22} &= 8\gamma_{XYZU}^2 + 2\gamma_{XYZU}(\mathfrak{S}(\gamma_U) + 2\mathfrak{S}(\gamma_{XU}) + 4\mathfrak{S}(\gamma_{XYU})) \\ &\quad + 4\mathfrak{S}(\gamma_{XYU}\gamma_{XYZ}) + 2\mathfrak{S}(\gamma_{XU}\gamma_{XYZ}) \\ &\quad + \mathfrak{S}(\gamma_{XZ}\gamma_{YU}) + \mathfrak{S}(\gamma_U\gamma_{XYZ}),\end{aligned}\quad (26)$$

$$\begin{aligned}e_{32} &= 46\gamma_{XYZU}\mathfrak{S}(\gamma_{XZ}\gamma_{YU}) + 48\mathfrak{S}(\gamma_{XYZ}\gamma_{XZU}\gamma_{YU}) \\ &\quad + 2\gamma_{XYZU}(2\mathfrak{S}(\gamma_U\gamma_X) + 8\mathfrak{S}(\gamma_U\gamma_{XY}) + 15\mathfrak{S}(\gamma_U\gamma_{XYZ}))\end{aligned}$$

$$\begin{aligned}
& + 16\mathfrak{S}(\gamma_U \gamma_{XYU} \gamma_{XYZ}) + 12\mathfrak{S}(\gamma_U \gamma_{XYZ}^2) \\
& + 24\mathfrak{S}(\gamma_{XZU} (\gamma_{XY} \gamma_{YU} + \gamma_{XU} \gamma_{YZ})) + 12\mathfrak{S}(\gamma_{XU} \gamma_{XZ} \gamma_{YU}) \\
& + 6\mathfrak{S}(\gamma_{XZ}^2 \gamma_{YU}) + 8\mathfrak{S}(\gamma_U \gamma_{XU} \gamma_{XYZ}) + 12\mathfrak{S}(\gamma_U \gamma_{XY} \gamma_{XYZ}) \\
& + 8\mathfrak{S}(\gamma_U \gamma_{XYU} \gamma_{XZ}) + 6\mathfrak{S}(\gamma_U \gamma_{XY} \gamma_{XZ}) + \mathfrak{S}(\gamma_U^2 \gamma_{XYZ}) \\
& + 4\mathfrak{S}(\gamma_U \gamma_{XZ} \gamma_{YU}) + 4\mathfrak{S}(\gamma_U \gamma_X \gamma_{XYZ}) \\
& + 3\mathfrak{S}(\gamma_U \gamma_{XZ} \gamma_Y), \tag{27}
\end{aligned}$$

$$\begin{aligned}
e_{42} = & 46\mathfrak{S}(\gamma_U \gamma_{XYZ}) \mathfrak{S}(\gamma_{XZ} \gamma_{YU}) + 16\mathfrak{S}(\gamma_U \gamma_{XYZ} \gamma_{XZU} \gamma_Y) \\
& + 48\mathfrak{S}(\gamma_U \gamma_{XYU} \gamma_{XZ} \gamma_{YZ}) + 92\mathfrak{S}(\gamma_{XU} \gamma_{XZ} \gamma_{YU} \gamma_{YZ}) \\
& + 14\gamma_{XYZU} \mathfrak{S}(\gamma_U \gamma_{XZ} \gamma_Y) + 4\mathfrak{S}(\gamma_U^2 \gamma_{XYZ}^2) \\
& + 22\mathfrak{S}(\gamma_{XZ}^2 \gamma_{YU}^2) + 8\mathfrak{S}(\gamma_U \gamma_{XU} \gamma_{XYZ} \gamma_Y) \\
& + 4\mathfrak{S}(\gamma_U^2 \gamma_{XY} \gamma_{XYZ}) + 24\mathfrak{S}(\gamma_U \gamma_{XY} \gamma_{XZ} \gamma_{YU}) \\
& + 48\mathfrak{S}(\gamma_U \gamma_{XY} \gamma_{XZ} \gamma_{YZ}) + 8\mathfrak{S}(\gamma_U \gamma_{XYU} \gamma_{XZ} \gamma_Y) \\
& + 24\mathfrak{S}(\gamma_U \gamma_{XYZ} \gamma_{XZ} \gamma_Y) + 12\mathfrak{S}(\gamma_U \gamma_{XZ}^2 \gamma_{YU}) \\
& + 4\mathfrak{S}(\gamma_U \gamma_X \gamma_{XYZ} \gamma_Y) + 4\mathfrak{S}(\gamma_U \gamma_X \gamma_{XZ} \gamma_{YU}) \\
& + 12\mathfrak{S}(\gamma_U \gamma_{XU} \gamma_{XZ} \gamma_Y) + 2\mathfrak{S}(\gamma_U^2 \gamma_{XY} \gamma_{XZ}) \\
& + 4\mathfrak{S}(\gamma_U \gamma_{XZ} \gamma_Y \gamma_{YU}) + 12\mathfrak{S}(\gamma_U \gamma_{XZ}^2 \gamma_Y) \\
& + 6\mathfrak{S}(\gamma_U \gamma_X \gamma_{XZ} \gamma_Y) + \mathfrak{S}(\gamma_U^2 \gamma_{XZ} \gamma_Y) \\
& + 6\gamma_U \gamma_X \gamma_Y \gamma_Z, \tag{28}
\end{aligned}$$

$$\begin{aligned}
e_{52} = & 14\mathfrak{S}(\gamma_U \gamma_{XU} \gamma_{XZ} \gamma_Y \gamma_{YZ}) + 8\mathfrak{S}(\gamma_U^2 \gamma_{XY} \gamma_{XZ} \gamma_{YZ}) \\
& + 6\mathfrak{S}(\gamma_U \gamma_{XZ}^2 \gamma_Y \gamma_{YU}) + 8\mathfrak{S}(\gamma_U \gamma_X \gamma_{XZ} \gamma_Y \gamma_{YZ}) \\
& + 2\mathfrak{S}(\gamma_U^2 \gamma_{XZ}^2 \gamma_Y) + 4\mathfrak{S}(\gamma_U \gamma_X \gamma_{XU} \gamma_Y \gamma_Z) \\
& + \gamma_U \gamma_X \gamma_Y \gamma_Z \mathfrak{S}(\gamma_U), \tag{29}
\end{aligned}$$

$$\begin{aligned}
e_{44} = & 24\gamma_{XYZU} (\mathfrak{S}(\gamma_U \gamma_X \gamma_Y) + 2\mathfrak{S}(\gamma_U \gamma_{XZ} \gamma_Y)) \\
& + 48\mathfrak{S}(\gamma_U \gamma_{XYU} \gamma_{XZ} \gamma_{YZ}) + 46\mathfrak{S}(\gamma_U \gamma_{XYZ}) \mathfrak{S}(\gamma_{XZ} \gamma_{YU}) \\
& + 46\mathfrak{S}(\gamma_U \gamma_{XYZ} \gamma_{XZU} \gamma_Y) + 46\mathfrak{S}(\gamma_{XU} \gamma_{XZ} \gamma_{YU} \gamma_{YZ}) \\
& + 11\mathfrak{S}(\gamma_U^2 \gamma_{XYZ}^2) + 11\mathfrak{S}(\gamma_{XZ}^2 \gamma_{YU}^2) + 12\mathfrak{S}(\gamma_U^2 \gamma_{XY} \gamma_{XYZ}) \\
& + 24\mathfrak{S}(\gamma_U \gamma_{XU} \gamma_{XYZ} \gamma_Y) + 24\mathfrak{S}(\gamma_U \gamma_{XY} \gamma_{XZ} \gamma_{YU}) \\
& + 24\mathfrak{S}(\gamma_U \gamma_{XY} \gamma_{XZ} \gamma_{YZ}) + 24\mathfrak{S}(\gamma_U \gamma_{XYU} \gamma_{XZ} \gamma_Y) \\
& + 24\mathfrak{S}(\gamma_U \gamma_{XYZ} \gamma_{XZ} \gamma_Y) + 12\mathfrak{S}(\gamma_U \gamma_{XZ}^2 \gamma_{YU}) \\
& + 12\mathfrak{S}(\gamma_U \gamma_X \gamma_{XYZ} \gamma_Y) + 12\mathfrak{S}(\gamma_U \gamma_X \gamma_{XZ} \gamma_{YU}) \\
& + 6\mathfrak{S}(\gamma_U^2 \gamma_X \gamma_{XYZ}) + 12\mathfrak{S}(\gamma_U \gamma_{XU} \gamma_{XZ} \gamma_Y) \\
& + 6\mathfrak{S}(\gamma_U^2 \gamma_{XY} \gamma_{XZ}) + 12\mathfrak{S}(\gamma_U \gamma_{XZ} \gamma_Y \gamma_{YU}) \\
& + 6\mathfrak{S}(\gamma_U \gamma_{XZ}^2 \gamma_Y) + 6\mathfrak{S}(\gamma_U \gamma_X \gamma_{XZ} \gamma_Y) \\
& + 3\mathfrak{S}(\gamma_U^2 \gamma_{XZ} \gamma_Y) + 3\gamma_U \gamma_X \gamma_Y \gamma_Z, \tag{30}
\end{aligned}$$

$$\begin{aligned}
e_{54} = & \gamma_U \gamma_X \gamma_Y \gamma_Z (9\mathfrak{S}(\gamma_U) + 48\mathfrak{S}(\gamma_{XYU}) + 42\gamma_{XYZU}) \\
& + 94\mathfrak{S}(\gamma_U \gamma_X \gamma_{XZU} \gamma_Y \gamma_{YZ}) + 142\mathfrak{S}(\gamma_U \gamma_{XU} \gamma_{XZ} \gamma_Y \gamma_{YZ}) \\
& + 72\mathfrak{S}(\gamma_U^2 \gamma_{XY} \gamma_{XZ} \gamma_{YZ}) + 46\mathfrak{S}(\gamma_U^2 \gamma_{XYZ} \gamma_{XZ} \gamma_Y) \\
& + 70\mathfrak{S}(\gamma_U \gamma_{XZ}^2 \gamma_Y \gamma_{YU}) + 12\mathfrak{S}(\gamma_U^2 \gamma_X \gamma_{XYZ} \gamma_Y) \\
& + 48\mathfrak{S}(\gamma_{XZ} \gamma_{YU}) \mathfrak{S}(\gamma_U \gamma_X \gamma_Y) + 72\mathfrak{S}(\gamma_U \gamma_X \gamma_{XZ} \gamma_Y \gamma_{YZ}) \\
& + 24\mathfrak{S}(\gamma_U^2 \gamma_{XY} \gamma_{XZ} \gamma_Y) + 18\mathfrak{S}(\gamma_U^2 \gamma_{XZ}^2 \gamma_Y) \\
& + 3\mathfrak{S}(\gamma_U^2 \gamma_{XZ} \gamma_Y^2) + 36\mathfrak{S}(\gamma_U \gamma_X \gamma_{XU} \gamma_Y \gamma_Z) \\
& + 12\mathfrak{S}(\gamma_U^2 \gamma_X \gamma_{XZ} \gamma_Y), \tag{31}
\end{aligned}$$

$$e_{64} = 40\gamma_U \gamma_X \gamma_Y \gamma_Z \mathfrak{S}(\gamma_{XZ} \gamma_{YU}) + 22\mathfrak{S}(\gamma_U^2 \gamma_X \gamma_{XZ} \gamma_Y \gamma_{YZ})$$

$$\begin{aligned}
& + 5\mathfrak{S}(\gamma_U^2 \gamma_{XZ}^2 \gamma_Y^2) \\
& + \gamma_U \gamma_X \gamma_Y \gamma_Z (3\mathfrak{S}(\gamma_U \gamma_X) + 12\mathfrak{S}(\gamma_U \gamma_{XY})), \tag{32}
\end{aligned}$$

$$\begin{aligned}
e_{66} = & 6\gamma_U \gamma_X \gamma_Y \gamma_Z (19\mathfrak{S}(\gamma_U \gamma_{XYZ}) + 39\mathfrak{S}(\gamma_{XZ} \gamma_{YU})) \\
& + 120\mathfrak{S}(\gamma_U^2 \gamma_X \gamma_{XZ} \gamma_Y \gamma_{YZ}) + 30\mathfrak{S}(\gamma_U^2 \gamma_{XZ}^2 \gamma_Y^2) \\
& + 15\gamma_U \gamma_X \gamma_Y \gamma_Z (\mathfrak{S}(\gamma_U \gamma_X) + 4\mathfrak{S}(\gamma_U \gamma_{XY})) \\
& + 30\mathfrak{S}(\gamma_U^2 \gamma_X \gamma_{XZ} \gamma_Y^2), \tag{33}
\end{aligned}$$

$$\begin{aligned}
e_{76} = & 54\gamma_U \gamma_X \gamma_Y \gamma_Z \mathfrak{S}(\gamma_U \gamma_{XZ} \gamma_Y) \\
& + 15\gamma_U \gamma_X \gamma_Y \gamma_Z \mathfrak{S}(\gamma_U \gamma_X \gamma_Y), \tag{34}
\end{aligned}$$

$$e_{88} = 96\gamma_U^2 \gamma_X^2 \gamma_Y^2 \gamma_Z^2. \tag{35}$$

V. DISCUSSION

The two key consequences of the imperfection of the measurement apparatus on a cumulant-mapping measurement are immediately apparent from the general results above: First, the noise-induced contribution to the cumulant κ_n always appears in the second order of the average event rate ν_0 . For a given level of noise, there always exists a critical event rate $\nu_{n,\text{crit}}$, which should not be exceeded, to avoid contamination of the results:

$$\nu_{2,\text{crit}} = \frac{\epsilon}{\sigma^2} \frac{\gamma_{XY}}{\gamma_X \gamma_Y} \tag{36}$$

$$\nu_{3,\text{crit}} = \frac{\epsilon}{\sigma^2} \frac{\gamma_{XYZ}}{\mathfrak{S}(\gamma_{XZ} \gamma_Y)} \tag{37}$$

$$\nu_{4,\text{crit}} = \frac{\epsilon}{\sigma^2} \frac{\gamma_{XYZU}}{\mathfrak{S}(\gamma_U \gamma_{XYZ}) + \mathfrak{S}(\gamma_{XZ} \gamma_{YU})} \tag{38}$$

where ϵ is the permissible fraction of the false-cumulant events relative to the true-cumulant signal.

Second, the external noise could potentially lead to an increase in the width of the distribution, given by the square root of the corresponding variance, from which the cumulant is sampled. In a perfect apparatus, the width of the distribution for κ_n grows generally as $\nu_0^{n/2}$ with the average event rate. If no restrictions are imposed on the event rate, the fastest-growing noise-induced contribution raises as $\nu_0^n \sigma^n$, and will eventually dominate the distribution width. If the event rate is held under the critical $\nu_{n,\text{crit}}$, the product $\nu_0 \sigma^2$ is bounded by a constant (See eqs. (36) to (38)), and the effective noise-induced width grows as $\nu_0^{n/2}$ as well. The final distribution width then depends on the specific parameters.

The high-order dependence of the distribution width for κ_n with $n \geq 3$ on the event rate leads to a paradoxical situation in a cumulant-mapping measurement, where higher event rate increases the number of events observed in a given length of time – yet the measurement becomes *less* accurate, due to the faster broadening of the cumulant distribution.

We will now turn to some specific, representative measurement regimes. We will consider three scenarios: A dominant process with no background (subsection V.1), a minor process on a strong background (subsection V.2), and a minor process, where *one* of the fragments is

background-free (subsection V.3). For simplicity, and unless stated otherwise, we will assume unit detection efficiency throughout ($\beta_x = \beta_y = \beta_z = \beta_v = 1$). Due to the linear relationship between the intrinsic (α) and detector-based (p) elementary-event probabilities, a choice of $\beta < 1$ amounts to a redefinition of the events, provided that none of the detection probabilities vanish – see the discussion following Eq. (7) – and leaves the conclusions qualitatively unaffected. Furthermore, we set both the permissible contamination threshold ϵ and the noise level σ at 1%.

V.1. A dominant process

Here, we assume that every primitive event produces all fragments of interest, with a unit probability. All these fragments are reliably detected, and no other fragmentation processes occur in the system. This scenario could be seen as an idealized model of the Coulomb explosion. Under our assumptions, all γ parameters take unit value (See eq. (6)). Equations (9) to (12), (21) and (22) then take the much-simplified form:

$$\kappa_2 \stackrel{\text{dm}}{=} \nu_0 + \nu_0^2 \sigma^2, \quad (39)$$

$$\kappa_3 \stackrel{\text{dm}}{=} \nu_0 + 3\nu_0^2 \sigma^2, \quad (40)$$

$$\kappa_4 \stackrel{\text{dm}}{=} \nu_0 + 7\nu_0^2 \sigma^2, \quad (41)$$

$$\text{Var } \kappa_2 \stackrel{\text{dm}}{=} \nu_0 + 2\nu_0^2 + 7\nu_0^2 \sigma^2 + 4\nu_0^3 \sigma^2 + 2\nu_0^4 \sigma^4, \quad (42)$$

$$\begin{aligned} \text{Var } \kappa_3 \stackrel{\text{dm}}{=} & \nu_0 + 24\nu_0^2 + 15\nu_0^3 + 31\nu_0^2 \sigma^2 \\ & + 174\nu_0^3 \sigma^2 + 45\nu_0^4 \sigma^2 + 186\nu_0^4 \sigma^4 \\ & + 45\nu_0^5 \sigma^4 + 15\nu_0^6 \sigma^6, \end{aligned} \quad (43)$$

$$\begin{aligned} \text{Var } \kappa_4 \stackrel{\text{dm}}{=} & \nu_0 + 118\nu_0^2 + 484\nu_0^3 + 96\nu_0^4 + 127\nu_0^2 \sigma^2 \\ & + 2380\nu_0^3 \sigma^2 + 3796\nu_0^4 \sigma^2 + 5054\nu_0^4 \sigma^4 \\ & + 384\nu_0^5 \sigma^2 + 7260\nu_0^5 \sigma^4 + 576\nu_0^6 \sigma^4 \\ & + 3948\nu_0^6 \sigma^6 + 384\nu_0^7 \sigma^6 + 96\nu_0^8 \sigma^8. \end{aligned} \quad (44)$$

The key properties of the covariant mapping in this case are illustrated in Figure 2, for $\kappa_n, n = 2, 3, 4$. In all three cases, the expectation of the cumulant grows almost perfectly linearly with the average event rate, at least until $\nu_0 = 50$ (Panel a). The contribution from the noise-induced, false covariance remains small, on the level of a few percent (Panel b). Our chosen contamination tolerance of 1% is reached at $\nu_{2,\text{crit}} = 14.3$, $\nu_{3,\text{crit}} = 33.3$, and $\nu_{4,\text{crit}} = 100$. If higher contamination levels are permissible, then even higher even rates are possible. The noise contribution to the variance is even smaller at these events rates (Panel c).

A practically important property of the cumulant is the ratio of the width of the distribution of the sampled expectation and the expectation itself, which determines the experimental accuracy. For a measurement with N

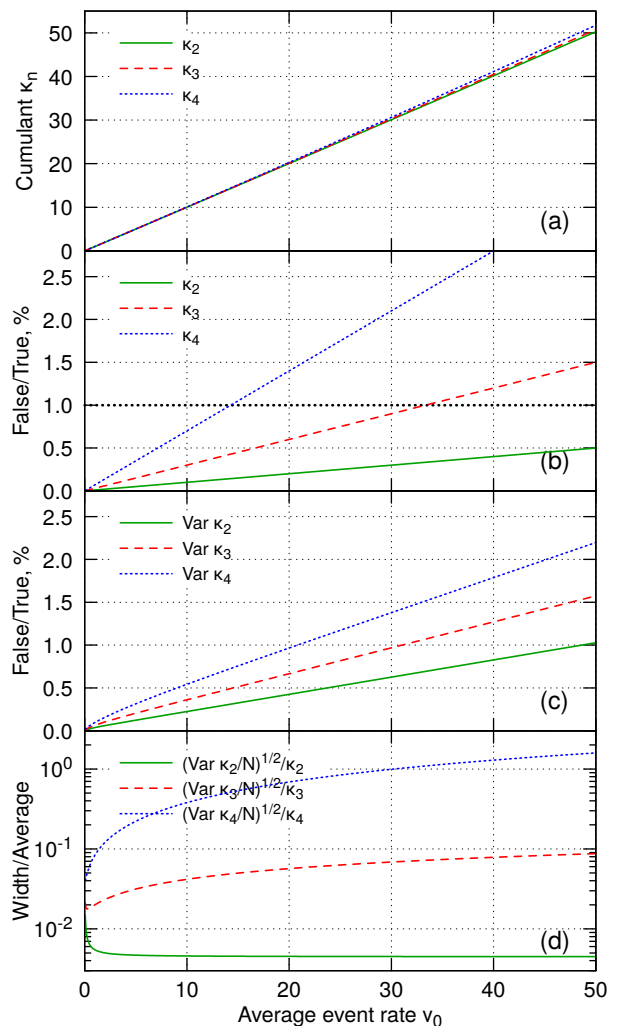


FIG. 2. Dominant process with no background (section V.1), $\gamma_a = 1$, noise level $\sigma = 1\%$, $N = 10^5$ shots. Green solid line: covariance (2-cumulant) κ_2 . Red dashed line: 3-cumulant κ_3 . Blue dotted line: 4-cumulant κ_4 . Panel (a): total value of the cumulant, as a function of the average event rate ν_0 . Panel (b): the ratio of the false (noise-induced) and true contributions to the cumulant in percent. Panel (c): the ratio of the false and true contributions to the cumulant variance. Panel (d): Measurement uncertainty r_n , eq. (45).

shots, the relative width r_n is given by:

$$r_n = \frac{1}{\kappa_n} \sqrt{\frac{1}{N} \text{Var } \kappa_n}. \quad (45)$$

This quantity is plotted in Figure 2d for $N = 10^5$. As expected, the 2-cumulant (the covariance) shows a behavior qualitatively different from the higher cumulants: The r_2 decreases, essentially monotonously, reaching the asymptote of about 0.014 at $\nu_0 > 50$. In contrast, the r_3 and r_4 reach a minimum at, respectively, $\nu_0 = 0.26$ and $\nu_0 = 0.045$. Asymptotically, both grow without a bound, respectively linearly and quadratically with ν_0 .

At the critical event rate $\nu_{n,\text{crit}}$, we obtain $r_3 = 0.23$ and $r_4 = 1.6$, so that the width of the distribution is comparable to the magnitude of the cumulant. As the result, a number of shots much higher than 10^5 is likely necessary to obtain accurate results for higher cumulants in this case.

Overall, the Coulomb explosion appears to be the ideal case for applications of the cumulant mapping[20], even in the presence of moderate noise levels.

V.2. A minor process

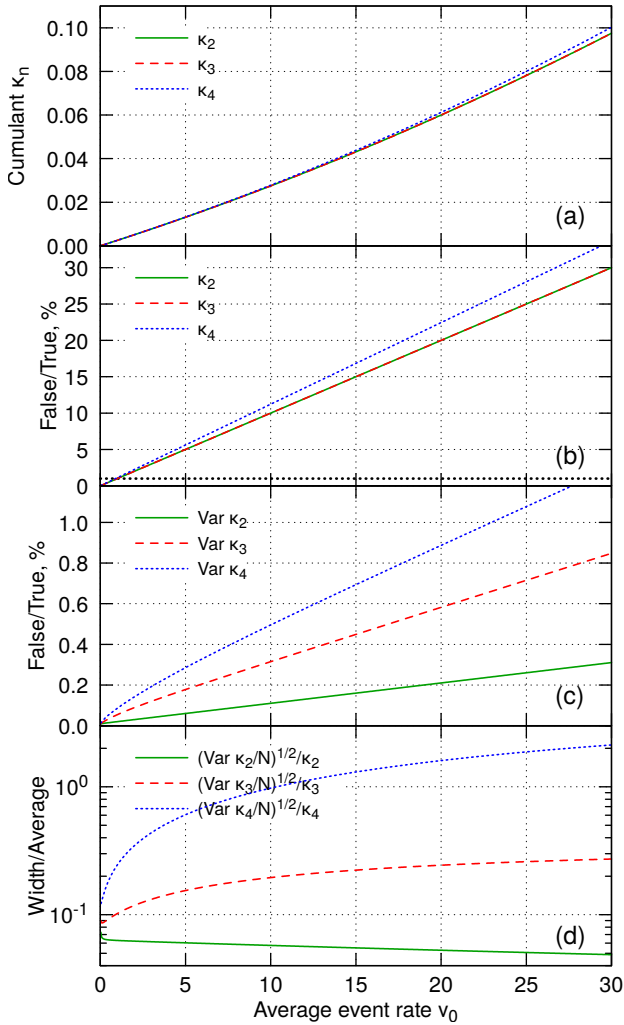


FIG. 3. Minor process with strong, correlated background (section V.2), $\tau = 2.5 \times 10^{-3}$, noise level $\sigma = 1\%$, $N = 10^7$ shots. Also see Fig. 2 for panel description.

Our second hypothetical scenario involves a minor channel of interest, which occurs in a fraction τ ($\tau \ll 1$) of the primitive fragmentation events. For illustrative purposes, we choose $\tau = 0.25\%$. All other fragmentation

channels are assumed to occur with equal probability. For example, for the 3-cumulant, primitive fragmentation channels leading to fragments X, Y, Z, X + Y, X + Z, and Y + Z are taken to be equally probable, at $\frac{1}{6}(1 - \tau) \approx 16.6\%$. The number of shots is now $N = 10^7$. For our choice, the background is *partially* correlated: The events producing X, Y, and Z alone form the uncorrelated part of the background, as considered by Frasiniski[19]. On the other hand, events producing fragment pairs form the correlated background. Both correlated and uncorrelated background induce false-cumulant contributions in the presence of noise, but, as will be seen shortly, with a dramatically different efficiency.

The cumulants are now given by:

$$\kappa_2^{\text{mc}} \approx \nu_0 \tau + \frac{1}{4} \nu_0^2 \sigma^2, \quad (46)$$

$$\kappa_3^{\text{mc}} \approx \nu_0 \tau + \frac{1}{4} \nu_0^2 \sigma^2, \quad (47)$$

$$\kappa_4^{\text{mc}} \approx \nu_0 \tau + \frac{55}{196} \nu_0^2 \sigma^2. \quad (48)$$

The true-cumulant contribution, linear in ν_0 , is proportional to the primitive event rate τ , as expected. However, the false-cumulant term is τ -independent. As the result, the total cumulant (Fig. 3a) now visibly deviates from linear dependence on ν_0 . The false-cumulant contribution reaches 30% already at the $\nu_0 = 30$ average event rate. Our chosen critical threshold of 1% false-cumulant contamination is reached at $\nu_0 \approx 1$, in all three cases. At such low event rates, coincidence detection, which is immune to noise for high detection efficiencies[23], is likely the preferred detection mode.

The full expressions for $\text{Var } \kappa_n$ are somewhat lengthy[31], but for our choice of parameters and $\nu_0 \leq 30$, they are adequately approximated by:

$$\text{Var } \kappa_2^{\text{mc}} \approx 0.250 \nu_0^2, \quad (49)$$

$$\text{Var } \kappa_3^{\text{mc}} \approx 0.417 \nu_0^2 + 0.246 \nu_0^3, \quad (50)$$

$$\text{Var } \kappa_4^{\text{mc}} \approx 0.770 \nu_0^2 + 2.61 \nu_0^3 + 0.467 \nu_0^4. \quad (51)$$

As before, the variances are dominated by the true-cumulant contribution, with less than 1.5% stemming from the noise for $\nu_0 \leq 30$ (Fig. 3c). Finally, the relative width of the distribution (Fig. 3d) follows the same trend as before: the $\text{Var } \kappa_2$ monotonously decreases in the region of interest, while $\text{Var } \kappa_3$ ($\text{Var } \kappa_4$) reaches a minimum at $\nu_0 = 0.10$ ($\nu_0 = 0.12$) and increases linearly (quadratically) for large ν_0 .

This scenario is clearly unfavorable to cumulant detection, with either very low average event rates, or exceptionally high stability of the experimental setup being essential. The reason behind this, somewhat disappointing outcome, is the partially-correlated nature of the dominant background. From eq. (11), the noise combines the one- and two-fragment correlations into false 3-particle cumulant. Similarly, the one- and three- and two separate two-particle correlations are noise-coupled to produce false 4-cumulant (eq. (21)). When the background

is already partially-correlated, even small levels of noise are sufficient to swamp the weak signal of interest.

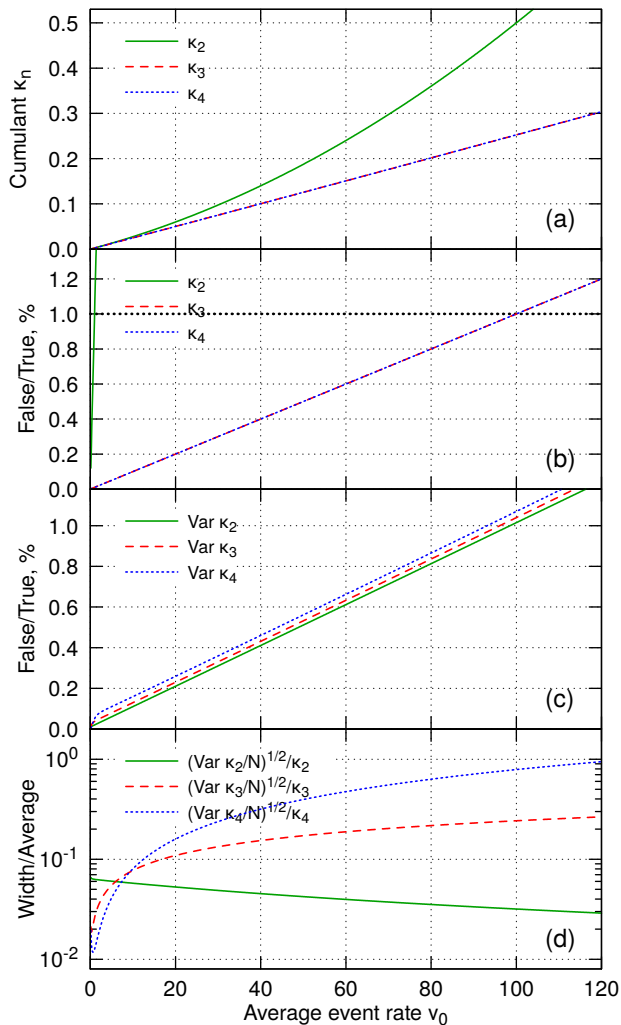


FIG. 4. Minor process with strong, but uncorrelated background (section V.2), $\tau = 2.5 \times 10^{-3}$, noise level $\sigma = 1\%$, $N = 10^7$ shots. Also see Fig. 2 for panel description.

For higher cumulants (but not for the 2-particle covariance, for which this scenario is identical to the correlated-background case), the situation changes dramatically if the background is strong, but uncorrelated (See Fig. 4). Now, the primitive fragmentation event is assumed to lead to either the 2-/3-/4-particle fragmentation (probability τ), or to only *one* of the fragments, each with an equal probability $(1 + (n-1)\tau)/n$ ($n = 2, 3, 4$). The 3- and 4-cumulants are now given by:

$$\kappa_{3,4}^{\text{mu}} \approx \nu_0 \tau + \nu_0^2 \sigma^2 \tau, \quad (52)$$

so that *both* the true- and the false-cumulants are now proportional to the desired-event rate τ . In the relevant range of ν_0 , the variances behave approximately like:

$$\text{Var } \kappa_3^{\text{mu}} \approx 0.037 \nu_0^3, \quad (53)$$

$$\text{Var } \kappa_4^{\text{mu}} \approx 0.00391 \nu_0^4. \quad (54)$$

The 3- and 4-cumulants are now essentially linear in ν_0 , for event rates up to several hundred. In contrast, the κ_2 is nearly-perfectly quadratic, and is dominated by the false covariance (Fig. 4a). The critical event rate for $\kappa_{3,4}$ is now reached at $\nu_0 = 100$ (Fig. 4b), while the noise-induced contributions to the variances remain small in this range (Fig. 4c). The behavior of the relative width of the distribution of κ (Fig. 4d) remains qualitatively the same, with the optimal width reached for very low event rates: $\nu_0 = 0.26$ ($\nu_0 = 0.65$) for κ_3 (κ_4).

Thus, the nature of the background events plays a critical role for applications of higher-cumulant mapping to minor channels. As long as the background remains perfectly uncorrelated, the cumulant signal remains reliable for very high event rates. On the other hand, presence of already moderate two-particle correlated background interferes with both 3- and 4-cumulant.

V.3. A minor process with a marker fragment

Our final scenario reflects a not uncommon situation, where *one* of the fragments comes exclusively from the process of interest, and is background-free. Other fragments appear on top of a strong, correlated background. All present background fragmentation pathways taken as equally likely, similar to Section V.2 above. Thus, the background-free fragment serves as a “marker” of the process of interest. Under the same assumptions as in Section V.2, the n -cumulants now become:

$$\kappa_2^{\text{mt}} \approx \nu_0 \tau + \nu_0^2 \sigma^2 \tau, \quad (55)$$

$$\kappa_3^{\text{mt}} \approx \nu_0 \tau + \frac{5}{3} \nu_0^2 \sigma^2 \tau, \quad (56)$$

$$\kappa_4^{\text{mt}} \approx \nu_0 \tau + \frac{19}{7} \nu_0^2 \sigma^2 \tau, \quad (57)$$

so that both the true- and false-cumulant contributions are proportional to the desired event’s probability τ . This is an extremely favorable situation: the critical event rate ν_{crit} does not depend on how small τ is. For our chosen 1% noise level and false-cumulant tolerance, $\nu_{2,\text{crit}} = 100$, $\nu_{3,\text{crit}} = 60$, and $\nu_{4,\text{crit}} = 37$ (See Fig. 5b).

The variances of the cumulant are also proportional to τ in this scenario. Keeping only the terms relevant below the critical event rate, we obtain:

$$\text{Var } \kappa_2^{\text{mt}} \approx \nu_0^2 \tau, \quad (58)$$

$$\text{Var } \kappa_3^{\text{mt}} \approx 4.33 \nu_0^2 \tau + 0.668 \nu_0^3 \tau, \quad (59)$$

$$\text{Var } \kappa_4^{\text{mt}} \approx 11.8 \nu_0^3 \tau + 0.658 \nu_0^4 \tau. \quad (60)$$

The false-cumulant contribution to the variance, again, remains small (Fig. 5c). For our chosen parameters, the relative widths of the κ_n distributions follow the same

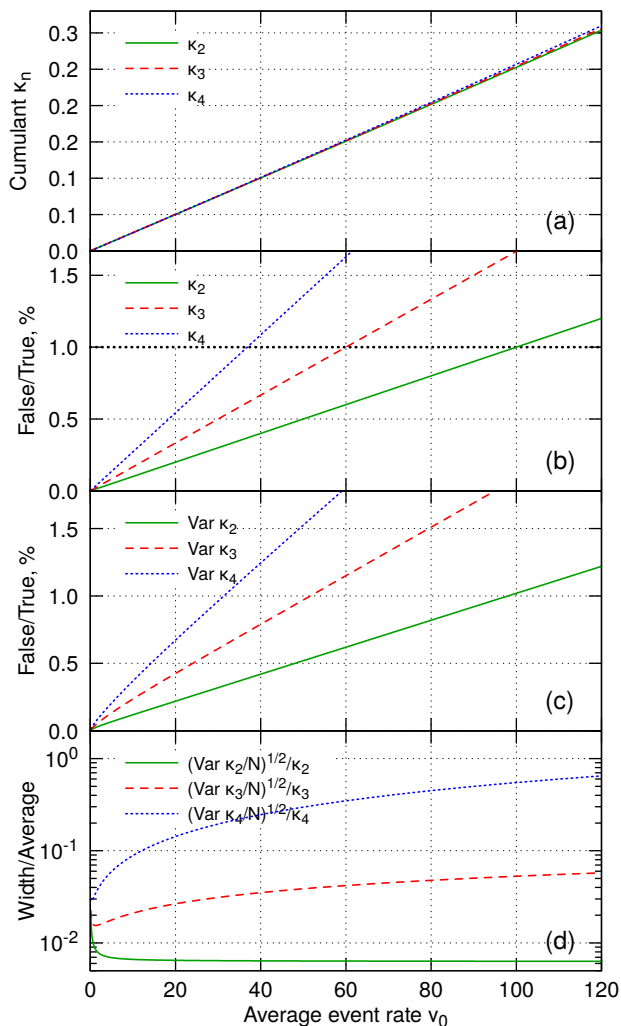


FIG. 5. Minor process with strong, correlated background and one, background-free (marker) fragment channel (section V.3), $\tau = 2.5 \times 10^{-3}$, noise level $\sigma = 1\%$, $N = 10^7$ shots. Also see Fig. 2 for panel description.

pattern seen for the dominant-contribution case (Section V.1 above). Quantity $\sqrt{\text{Var } \kappa_2}/\kappa_2$ goes to zero as $\nu_0^{-1/2}$ with increasing ν_0 . In contrast, $\sqrt{\text{Var } \kappa_{3,4}}/\kappa_{3,4}$ grow as $\nu_0^{1/2}$ and $\nu_0^{3/2}$ asymptotically (Fig. 5d). Their minima are again found at low ν_0 (1.2 and 0.3, respectively).

Thus, the presence of a background-free fragment in a minor fragmentation channel makes cumulant mapping robust with respect to moderate noise levels.

VI. CONCLUSIONS AND PERSPECTIVE

In this work, we have introduced the statistical analysis of cumulant mapping[19] in an imperfect experimen-

tal setup, where external noise sources introduce spurious, “false” correlations, and therefore “pollutes” the cumulant signal between fragments. Even at low noise levels, characteristic of a well-designed laboratory apparatus and laser systems (ca. 1%), false-cumulant contribution can contaminate the signal of interest, especially in a precision experiment. Minor fragmentation channels appearing on a partially-correlated background (Section V.2) are particularly affected. Coincidence detection is to be recommended in such situations. On the other hand, for prominent channels cumulant mapping offers significant advantages even in the presence of moderate external noise (Section V.1). A particularly interesting scenario, for which cumulant mapping is eminently suitable, is the situation where *one* of the fragments is background-free (Section V.3). There, very high average event rates are possible, while keeping false-cumulant contamination under control.

Our analysis shows that the external noise is an important factor for the cumulant-mapping technique, which needs to be carefully considered in the analysis of the results. At the very least, we recommend that the linear relationship between the cumulant signal and the average event rate should always be verified in an experimental measurement, e.g. by varying the target density or laser power. Deviations from linearity are strongly indicative of the severe false-cumulant contamination. For highly-variable light sources, binning techniques are a popular approach for dealing with the external noise[26, 27]. There, the characteristics of the process must be carefully considered when choosing the bin sizes. As we demonstrate, even 1% bins may lead to false-cumulant contamination in unfavorable cases.

Although we have tried to consider some representative measurement scenarios, they obviously cannot exhaust the full richness of this problem. The general expressions we provide (eqs. (9) to (12), (21) and (22)) can be used in many additional situations. For still more complicated cases, we include analytical tools[31], which can be adapted to the desired scenario.

ACKNOWLEDGMENT

J.M. gratefully acknowledges funding from the European Research Council (ERC) under the European Union’s Horizon 2020 research and innovation programme within a Consolidator Grant (CoG Agreement 101003142) and from the German Research Foundation (DFG) within a Heisenberg professorship.

- [1] L. J. Frasinski, K. Codling, and P. A. Hatherly, *Science* **246**, 1029 (1989).
- [2] A. E. Boguslavskiy, J. Mikosch, A. Gijsbertsen, M. Spanner, S. Patchkovskii, N. Gador, M. J. J. Vrakking, and A. Stolow, *Science* **335**, 1336 (2012).
- [3] B. Brehm and E. von Puttkamer, *Z. Naturforsch.* **A 22**, 8 (1967).
- [4] C. Vallance, D. Heathcote, and J. W. L. Lee, *J. Phys. Chem. A* **125**, 1117 (2021).
- [5] S. W. Crane, J. W. L. Lee, and M. N. R. Ashfold, *Phys. Chem. Chem. Phys.* **24**, 18830 (2022).
- [6] G. A. Cooper, S. T. Alavi, W. Li, S. K. Lee, and A. G. Suits, *J. Phys. Chem. A* **125**, 5481 (2021).
- [7] F. Allum, N. Anders, M. Brouard, P. Bucksbaum, M. Burt, B. Downes-Ward, S. Grundmann, J. Harries, Y. Ishimura, H. Iwayama, L. Kaiser, E. Kukuk, J. Lee, X. Liu, R. S. Minns, K. Nagaya, A. Niozu, J. Niskanen, J. O'Neal, S. Owada, J. Pickering, D. Rolles, A. Rudenko, S. Saito, K. Ueda, C. Vallance, N. Werby, J. Woodhouse, D. You, F. Ziaee, T. Driver, and R. Forbes, *Faraday Disc.* **228**, 571 (2021).
- [8] F. Allum, V. Music, L. Inhester, R. Boll, B. Erk, P. Schmidt, T. M. Baumann, G. Brenner, M. Burt, V. P. Demekhin, S. Doerner, A. Ehresmann, A. Galler, P. Grychtol, D. Heathcote, D. Kargin, M. Larsson, J. W. L. Lee, Z. Li, B. Manschwetus, L. Marder, R. Mason, M. Meyer, H. Otto, C. Passow, R. Pietschnig, D. Ramm, K. Schubert, L. Schwob, R. D. Thomas, C. Vallance, I. Vidanovic, C. von Korff Schmising, R. Wagner, P. Walter, V. Zhaunerchyk, D. Rolles, S. Bari, M. Brouard, and M. Ilchen, *Comm. Chem.* **5**, 2399 (2022).
- [9] J. W. McManus, T. Walmsley, K. Nagaya, J. R. Harries, Y. Kumagai, H. Iwayama, M. N. R. Ashfold, M. Britton, P. H. Bucksbaum, B. Downes-Ward, T. Driver, D. Heathcote, P. Hockett, A. J. Howard, E. Kukuk, J. W. L. Lee, Y. Liu, D. Milesevich, R. S. Minns, A. Niozu, J. Niskanen, A. J. Orr-Ewing, S. Owada, D. Rolles, P. A. Robertson, A. Rudenko, K. Ueda, J. Unwin, C. Vallance, M. Burt, M. Brouard, R. Forbes, and F. Allum, *Phys. Chem. Chem. Phys.* **24**, 22699 (2022).
- [10] T. Walmsley, F. Allum, J. R. Harries, Y. Kumagai, S. Lim, J. McManus, K. Nagaya, M. Britton, M. Brouard, P. Bucksbaum, M. Fushitani, I. Gabalski, T. Gejo, P. Hockett, A. J. Howard, H. Iwayama, E. Kukuk, C.-S. Lam, R. S. Minns, A. Niozu, S. Nishimuro, J. Niskanen, S. Owada, W. O. Rasmus, D. Rolles, J. Somper, K. Ueda, J. Unwin, S.-I. Wada, J. L. Woodhouse, R. Forbes, M. Burt, and E. M. Warne, *J. Phys. B* **57**, 235101 (2024).
- [11] F. Allum, M. Burt, K. Amini, R. Boll, H.-J. Kockert, P. K. Olshin, S. Bari, C. Bomme, F. Brausse, B. C. de Miranda, S. Duesterer, B. Erk, M. Geleoc, R. Geneaux, A. S. Gentleman, G. Goldsztejn, R. Guillemin, D. M. P. Holland, I. Ismail, P. Johnsson, L. Journal, J. Kuepper, J. Lahl, J. W. L. Lee, S. Maclot, S. R. Mackenzie, B. Manschwetus, A. S. Mereshchenko, R. Mason, J. Palaudoux, M. N. Piancastelli, F. Penent, D. Rompotis, A. Rouzee, T. Ruchon, A. Rudenko, E. Savelyev, M. Simon, N. Schirmel, H. Stapelfeldt, S. Techert, O. Travnikova, S. Trippel, J. G. Underwood, C. Vallance, J. Wiese, F. Ziaee, M. Brouard, T. Marchenko, and D. Rolles, *J. Chem. Phys.* **149**, 204313 (2018).
- [12] J. Unwin, F. Allum, M. Britton, I. Gabalski, H. Bromberger, M. Brouard, P. H. Bucksbaum, T. Driver, N. Ekanayake, D. Garg, E. Gougoula, D. Heathcote, A. J. Howard, P. Hockett, D. M. P. Holland, S. Kumar, C.-S. Lam, J. W. L. Lee, J. McManus, J. Mikosch, D. Milesevich, R. S. Minns, C. C. Papadopoulou, C. Passow, W. O. Rasmus, A. Roeder, A. Rouzee, M. Schuurman, A. Simao, A. Stolow, A. Tulnoor, C. Vallance, T. Walmsley, D. Rolles, B. Erk, M. Burt, and R. Forbes, *Comm. Phys.* **6**, 2399 (2023).
- [13] G. Mogol, B. Kaufman, T. Weinacht, C. Cheng, and I. Ben-Itzhak, *Phys. Rev. Res.* **6**, 2643 (2024).
- [14] T. Walmsley, J. W. McManus, Y. Kumagai, K. Nagaya, J. Harries, H. Iwayama, M. N. R. Ashfold, M. Britton, P. H. Bucksbaum, B. Downes-Ward, T. Driver, D. Heathcote, P. Hockett, A. J. Howard, J. W. L. Lee, Y. Liu, E. Kukuk, D. Milesevich, R. S. Minns, A. Niozu, J. Niskanen, A. J. Orr-Ewing, S. Owada, P. A. Robertson, D. Rolles, A. Rudenko, K. Ueda, J. Unwin, C. Vallance, M. Brouard, M. Burt, F. Allum, and R. Forbes, *J. Phys. Chem. A* **128**, 4548 (2024).
- [15] J. W. McManus, F. Allum, J. Featherstone, C.-S. Lam, and M. Brouard, *J. Phys. Chem. A* **128**, 3220 (2024).
- [16] T. Driver, R. Pipkorn, V. Averbukh, L. J. J. Frasinski, J. P. P. Marangos, and M. Edelson-Averbukh, *J. Am. Soc. Mass Spectrom.* **34**, 1230 (2023).
- [17] C. Schouder, A. S. Chatterley, F. Calvo, L. Christiansen, and H. Stapelfeldt, *Struct. Dyn.* **6**, 044301 (2019).
- [18] L. Kranabetter, H. H. Kristensen, C. A. Schouder, and H. Stapelfeldt, *J. Chem. Phys.* **160**, 131101 (2024).
- [19] L. J. Frasinski, *Phys. Chem. Chem. Phys.* **24**, 20776 (2022).
- [20] C. Cheng, L. J. Frasinski, G. Mogol, F. Allum, A. J. Howard, D. Rolles, P. H. Bucksbaum, M. Brouard, R. Forbes, and T. Weinacht, *Phys. Rev. Lett.* **130**, 093001 (2023).
- [21] Å. Andersson, *Phys. Chem. Chem. Phys.* **25**, 32723 (2023).
- [22] C. Cheng, L. J. Frasinski, F. Allum, A. J. Howard, P. H. Bucksbaum, R. Forbes, and T. Weinacht, *Phys. Rev. A* **109**, 042802 (2024).
- [23] J. Mikosch and S. Patchkovskii, *Journal of Modern Optics* **60**, 1426 (2013).
- [24] J. Mikosch and S. Patchkovskii, *Journal of Modern Optics* **60**, 1439 (2013).
- [25] V. Zhaunerchyk, L. J. Frasinski, J. H. D. Eland, and R. Feifel, *Phys. Rev. A* **89**, 053418 (2014).
- [26] K. Li, J. Laksman, T. Mazza, G. Doumy, D. Kouliantanos, A. Picchiotti, S. Serkez, N. Rohringer, M. Ilchen, M. Meyer, and L. Young, *Comm. Phys.* **5**, 191 (2022).
- [27] K. Dingel, T. Otto, L. Marder, L. Funke, A. Held, S. Savio, A. Hans, G. Hartmann, D. Meier, J. Viefhaus, B. Sick, A. Ehresmann, M. Ilchen, and W. Helml, *Sci. Rep* **12**, 17809 (2022).
- [28] O. Kornilov, M. Eckstein, M. Rosenblatt, C. P. Schulz, K. Motomura, A. Rouzee, J. Klei, L. Foucar, M. Siano, A. Lübcke, F. Schapper, P. Johnsson, D. M. P. Holland, T. Schlathöller, T. Marchenko, S. Düsterer, K. Ueda, M. J. J. Vrakking, and L. J. Frasinski, *Journal of Physics*

- B: Atomic, Molecular and Optical Physics **46**, 164028 (2013).
- [29] T. Driver, B. Cooper, R. Ayers, R. Pipkorn, S. Patchkovskii, V. Averbukh, D. R. Klug, J. P. Marangos, L. J. Frasinski, and M. Edelson-Averbukh, Phys. Rev. X **10**, 041004 (2020).
- [30] Wolfram Research, Inc., “Mathematica, Version 12.1,” (2020), Champaign, IL.
- [31] See supplemental material at **URL TBD** for the Mathematica notebooks containing derivation and simplification of all the expressions in Section IV and special cases considered in Section V.